Statistical properties of the normalized ice particle size distribution.

Julien Delanoë, Alain Protat, Jacques Testud, Dominique Bouniol, A.J. Heymsfield, A. Bansemer, P.R.A. Brown, R.M. Forbes

Statistical properties of the normalized ice particle size distribution

Julien Delanoë, Alain Protat, Jacques Testud, and Dominique Bouniol
Institut Pierre-Simon Laplace, Centre d'Etudes des Environnements Terrestres et Planétaires, Vélizy, France

A. J. Heymsfield and A. Bansemer
National Center for Atmospheric Research, Boulder, Colorado, USA

P. R. A. Brown and R. M. Forbes
Meteorological Office, Reading, UK

Received 31 August 2004; revised 1 February 2005; accepted 25 March 2005; published 17 May 2005.

[1] Testud et al. (2001) have recently developed a formalism, known as the "normalized particle size distribution (PSD)", which consists in scaling the diameter and concentration axes in such a way that the normalized PSDs are independent of water content and mean volume-weighted diameter. In this paper we investigate the statistical properties of the normalized PSD for the particular case of ice clouds, which are known to play a crucial role in the Earth's radiation balance. To do so, an extensive database of airborne in situ microphysical measurements has been constructed. A remarkable stability in shape of the normalized PSD is obtained. The impact of using a single analytical shape to represent all PSDs in the database is estimated through an error analysis on the instrumental (radar reflectivity and attenuation) and cloud (ice water content, effective radius, terminal fall velocity of ice crystals, visible extinction) properties. This resulted in a roughly unbiased estimate of the instrumental and cloud parameters, with small standard deviations ranging from 5 to 12%. This error is found to be roughly independent of the temperature range. This stability in shape and its single analytical approximation implies that two parameters are now sufficient to describe any normalized PSD in ice clouds: the intercept parameter N_0^* and the mean volume-weighted diameter D_m. Statistical relationships (parameterizations) between N_0^* and D_m have then been evaluated in order to reduce again the number of unknowns. It has been shown that a parameterization of N_0^* and D_m by temperature could not be envisaged to retrieve the cloud parameters. Nevertheless, D_m-T and mean maximum dimension diameter -T parameterizations have been derived and compared to the parameterization of Kristjánsson et al. (2000) currently used to characterize particle size in climate models. The new parameterization generally produces larger particle sizes at any temperature than the Kristjánsson et al. (2000) parameterization. These new parameterizations are believed to better represent particle size at global scale, owing to a better representativity of the in situ microphysical database used to derive it. We then evaluated the potential of a direct N_0^*-D_m relationship. While the model parameterized by temperature produces strong errors on the cloud parameters, the N_0^*-D_m model parameterized by radar reflectivity produces accurate cloud parameters (less than 3% bias and 16% standard deviation). This result implies that the cloud parameters can be estimated from the estimate of only one parameter of the normalized PSD (N_0^* or D_m) and a radar reflectivity measurement.

Citation: Delanoë, J., A. Protat, J. Testud, D. Bouniol, A. J. Heymsfield, A. Bansemer, P. R. A. Brown, and R. M. Forbes (2005), Statistical properties of the normalized ice particle size distribution, *J. Geophys. Res.*, *110*, D10201, doi:10.1029/2004JD005405.

1. Introduction

[2] The knowledge of the cloud properties at global scale has been clearly identified as a mandatory step to reach if the operational weather and climate change forecasts are to be improved. The occurence of clouds at global scale in the tropospheric layer is indeed very large, and clouds significantly influence the Earth's shortwave and longwave radiation budget through scattering, absorption and emission. In the framework of the future space missions devoted to the monitoring of the microphysical, radiative, and dynamic properties of clouds at global scale using the cloud radar and lidar combination (the first one will be the so-called

0148-0227/05/2004JD005405

"Afternoon Train" mission), there is a need for new methodologies to derive the cloud properties from this new spaceborne instrumental synergy. Most cloud parameters that can be derived from ground-based, airborne, and spaceborne passive and active remote sensing refer to a volume sampled by the different instruments. The physical link between the cloud parameters and the measurements in this sampling volume is the particle size distribution (hereafter referred to as the PSD), that is, the statistical distribution of the cloud particle size in the sampled volume. In particular, the radar and lidar observables, as well as the microphysical and radiative properties of clouds, are directly functions of the PSD. As a result, any forward model between radar/lidar observables and cloud properties includes the statistical properties of the PSD [e.g., *Intrieri et al.*, 1993; *Donovan and van Lammeren*, 2001; *Tinel et al.*, 2005]. Unfortunately, it is well known that this PSD is highly variable in both liquid and ice phases, owing to variations over three to four decades of the water content in a single cloud, and the very different ranges of diameters encountered from one cloud to another. This high variability prevents from using a single analytical expression of the PSD to describe all clouds.

[3] *Testud et al.* [2001] (hereafter referred to as TAL01) have however recently proposed a formalism that allows a comparison of very different PSDs in the liquid part of precipitating systems. This formalism, known as the "normalized PSD", consists in scaling the diameter and concentration axes in such a way that the PSDs are independent of water content and mean volume-weighted diameter. TAL01 have extensively used this concept of normalized PSD on microphysical in situ measurements of tropical rain. They have shown that the shape of the normalized PSD was fairly stable, and that the convective and stratiform parts of tropical mesoscale convective systems were systematically characterized by roughly the same value of the intercept parameter of the normalized PSD. It followed from this important result that the statistical relationships between different moments of the PSD in rain (radar attenuation, rainfall, radar reflectivity, liquid water content, ...) were fairly invariant and resulted in a fairly accurate estimate of rainfall rate. This normalized PSD concept has then been applied with great success to the TRMM Mission (Tropical Rainfall Measuring Mission) in order to improve the rain rate estimate from the spaceborne precipitation radar [*Ferreira et al.*, 2001] and check out the consistency between the TRMM microwave imager and precipitation radar.

[4] Although it is well known that among the different types of clouds ice clouds play a crucial role in the Earth's radiation balance [e.g., *Stephens et al.*, 1990], the investigation of the statistical properties of the normalized ice cloud PSD, and the potential for establishment of robust statistical relationships between radar/lidar observables and cloud properties, had not been carried out yet. In the present study we will try to answer the following questions: does the stability of the PSD shape obtained for the liquid phase in precipitating systems by TAL01 also hold for ice clouds? Are the statistical properties of the normalized ice cloud PSD independent of temperature, type of ice cloud, and geographical location (midlatitude versus tropics)? If not, could these statistical properties be parameterized with some confidence as a function of the environmental parameters to which they are sensitive? Can we derive robust statistical relationships that can be used to derive the ice cloud properties from the new generation of active instruments (radars and lidars) or to represent clouds in large-scale models?

[5] In the present paper, we focus on the investigation of the statistical properties of the normalized ice cloud PSD using a very extensive database of airborne in situ microphysical measurements. In section 2, the normalized distribution concept is recalled. In section 3, the airborne in situ microphysical database is presented, as well as the methodology used to process them. In section 4, the statistical properties of the normalized ice cloud PSD are investigated. First, the stability of the PSD shape is evaluated. Then the statistical properties of the two parameters of the normalized PSD (namely, the intercept parameter and the mean-volume-weighted particle diameter, which are defined in section 2) are investigated, and different manners to parameterize them are evaluated. Our conclusions on the statistical properties of the normalized ice cloud PSD are then given in section 5.

2. Recall of the Normalized PSD Concept

2.1. Principle of the Normalization

[6] By definition, the particle size distribution N(D) is the number of particles per unit volume and per interval of diameter (m^{-4}), where D is the particle diameter (m). It is well known that this PSD is highly variable in both liquid and ice phases, owing to variations over three to four decades of the condensed water content in a single cloud, and the very different ranges of diameters encountered from one cloud to another. TAL01 have recently proposed a formalism that allows a comparison of very different PSDs in the liquid part of precipitating systems. This formalism, known as the "normalized PSD", consists in scaling the diameter and N(D) axes in such a way that the PSDs are independent of the liquid water content (LWC) and the mean volume-weighted diameter (D_m).

[7] Let us recall that LWC is proportional to the third moment of the PSD and D_m to the ratio of the fourth to the third moment of the PSD:

$$D_m = \frac{\int N(D) D^4 dD}{\int N(D) D^3 dD} \text{ in m} \tag{1}$$

$$LWC = \frac{\pi \rho_w}{6} \int N(D) D^3 dD \text{ in g.m}^{-3} \tag{2}$$

A general expression of the normalization of the PSD can be written as:

$$N(D) = N_0^* F(D/D_m) \tag{3}$$

where N_0^* is the scaling parameter for the concentration axis, D_m the scaling parameter for the diameter axis, and F(X) denotes the shape of the "normalized PSD".

[8] Assuming (1), then by definition F(X) satisfies the following equation:

$$\int_0^\infty F(X)X^4dX = \int_0^\infty F(X)X^3dX \quad (4)$$

Then, considering (2), we can also write:

$$\int_0^\infty F(X)X^3dX = \frac{6}{\pi\rho_w}\frac{LWC}{N_0^* D_m^4} \quad (5)$$

It follows from (4) and (5) that in order to make the normalized PSD independent of LWC and D_m, the third moment of the PSD must be constant. This constant has been chosen in such a way that the N_0^* parameter is equal to the intercept parameter N_0 of the exponential *Marshall and Palmer* [1948] PSD, which yields:

$$\int_0^\infty F(X)X^3dX = C = \frac{\Gamma(4)}{4^4} \quad (6)$$

As shown in TAL01, the N_0^* parameter is a function of LWC and D_m, which can be written as:

$$N_0^* = \frac{4^4}{\pi\rho_w}\frac{LWC}{D_m^4} \text{ in } m^4 \quad (7)$$

As discussed in the introduction section, our purpose here is to investigate the stability of the shape of the PSD in the case of ice clouds. To do so, however, the physical diameter of the crystals cannot be used directly, owing to a much higher complexity in particle types and shapes than for rain. Therefore, in order to adapt the mathematical formulation of TAL01, it has been chosen to use the convenient formulation of the "equivalent melted diameter" instead of the physical diameter, which corresponds to the diameter the ice particle would have if it was a spherical water particle of the same mass. This formulation implies that a density-diameter relationship must be assumed. This assumption will be further discussed in the next section.

[9] Using this definition of diameter, the formulation of the normalized ice PSD becomes:

$$N(D_{eq}) = N_0^* F(D_{eq}/D_m) \quad (8)$$

Regarding the analytical expression of the PSD shape, several mathematical formulations have been proposed (and are extensively used) in the literature. Given the particular shape of the normalized PSD for ice clouds, three formulations will be evaluated, which are described in the next subsection.

2.2. Analytical Formulations of the Normalized Ice PSD Shape

[10] It is generally proposed in the literature to use the exponential or gamma distribution as an analytical representation of the PSD shape, both for observational and modelling purposes. However, as will be shown in the next section, when the PSD is normalized, these analytical shapes result in a systematic underestimation of the concentration of the small ice particles, owing to the convexity of the normalized PSD tail. We have therefore considered an additional PSD shape, the so-called "modified gamma shape", which better describes the small particles. Below we review the general formulation of these analytical representations in a normalized framework. These analytical shapes will be used in the error analyses of section 4.

[11] The exponential shape: The exponential shape is the most widely used shape to describe raindrop size distributions, since the early works of *Marshall and Palmer* [1948]. After normalizing the exponential PSD, it may be written as:

$$F(D_{eq}/D_m) = \exp(-\Lambda D_{eq}/D_m) \quad (9)$$

TAL01 have shown that $\Lambda = 4$, and by construction of the normalization for an exponential PSD N_0^* is equal to N_0.

[12] The gamma μ shape, *Willis* [1984] and TAL01: This particular shape has the advantage of provide a more realistic characterization of coalescence growth and drop evaporation in numerical simulations. It has been first proposed by *Willis* [1984] to describe raindrop size distribution.

[13] This gamma-μ PSD may be written as

$$N(D) = N_0 D^\mu \exp(-\Lambda D) \quad (10)$$

where μ is a free parameter that can be variationally adjusted to the measured PSDs. Which after normalization expresses as:

$$\frac{N(D_{eq})}{N_0^*} = F_\mu\left(\frac{D_{eq}}{D_m}\right) = \frac{\Gamma(4)}{4^4}\cdot\frac{(4+\mu)^{4+\mu}}{\Gamma(4+\mu)}\cdot\left(\frac{D_{eq}}{D_m}\right)^\mu\cdot\exp\left[-(4+\mu)\frac{D_{eq}}{D_m}\right] \quad (11)$$

[14] The "modified gamma" shape [*Best*, 1950; *Law and Parsons*, 1943]: This shape has the advantage of well fitting the particular "S-shaped" structure of the ice cloud PSDs, where most data points are located. This modified gamma shape can be expressed as

$$N(D_{eq}) = N_0 D_{eq}^\alpha \exp(-kD_{eq}^\beta) \quad (12)$$

where α and β can be variationally adjusted to the measured PSDs.

[15] After normalization the PSD can be expressed as:

$$\frac{N(D_{eq})}{N_0^*} = F_{\alpha,\beta}\left(\frac{D_{eq}}{D_m}\right) = \beta\cdot\frac{\Gamma(4)}{4^4}\cdot\frac{\Gamma\left(\frac{\alpha+5}{\beta}\right)^{4+\alpha}}{\Gamma\left(\frac{\alpha+4}{\beta}\right)^{5+\alpha}} \cdot\left(\frac{D_{eq}}{D_m}\right)^\alpha\cdot\exp\left[-\left(\frac{D_{eq}}{D_m}\frac{\Gamma\left(\frac{\alpha+5}{\beta}\right)}{\Gamma\left(\frac{\alpha+4}{\beta}\right)}\right)^\beta\right] \quad (13)$$

2.3. Calculation Details

2.3.1. Density-Diameter Relationship

[16] It has been discussed previously that the physical diameter could not be used in the particular case of ice

clouds to compute the moments of the PSD, and it has been proposed to use the "equivalent-melted diameter" D_{eq}. In order to compute this equivalent melted diameter an assumption has to be made on the most representative ice density-diameter relationship. This problem of choosing a density-diameter relationship has been addressed recently in the literature. *Liu and Illingworth* [1999] have suggested that the *Brown and Francis* [1995] relationship, which is equivalent to the Locatelli and Hobbs relationship for "aggregates of unrimed radiating assemblages of plates, side planes, bullets and columns" [*Locatelli and Hobbs*, 1974] was realistic to describe midlatitude ice clouds. *Matrosov* [1996] used the Locatelli and Hobbs relationship, but assumed that particles less than 100 μm had the density of solid ice (i.e. 0.917g.cm^{-3}). More recently, *Gaussiat et al.* [2004] have shown using dual-wavelength radar observations that the *Brown and Francis* [1995] relationship reproduced their dual-wavelength observations, while others proposed in the literature did not. In addition, more generally *Field and Heymsfield* [2003] have highlighted that most parts of ice clouds were composed of aggregates. They have shown that for small ice particles, particle production (nucleation and/or break up) and diffusional growth govern the evolution of the PSD, while for larger particles the evolution of the PSD is dominated by aggregation.

[17] The *Brown and Francis* [1995]/*Locatelli and Hobbs* [1974] aggregates density-diameter relationship has therefore been used in the following. The particle density can be written as a function of the maximum bin diameter as

$$\rho(D) = 0.07D^{-1.1} \tag{14}$$

with ρ (D) in g cm^{-3} and D in mm.

[18] It is to mentioned that this relationship is not universal and should be not applied to describe all types of ice clouds. However, the purpose of this study is to evaluate the stability of the normalized PSD shape. Therefore, we have assumed a density-diameter relationship to work out this stability, and the sensitivity of this stability to the assumed particle type is then evaluated in a second step. As will be seen in the following, the results presented in this paper are not altered when different particle types are considered.

[19] Thus, assuming the density-diameter relationship (14), the equivalent-melted diameter D_{eq} can be computed as a function of the physical diameter and the ice density by considering the equivalent spherical water particle that has the same mass as the ice particle:

$$D_{eq} = (\rho(D)/\rho_w)^{1/3}D \tag{15}$$

2.3.2. Formulation of the Microphysical and Instrumental Parameters From the PSD

[20] For each measured spectrum we have computed the normalized PSD N (D_{eq}) and the different moments of the PSD that yield the instrumental (equivalent radar reflectivity Z_e, specific radar attenuation K) and microphysical (IWC, effective radius r_e, N_0^*, D_m, reflectivity-weighted terminal fall velocity Vt_Z, and visible extinction coefficient α) parameters. It is to be noted that the radar-related parameters (Z_e, Vt_Z, and K) have been calculated using a Mie scattering model. The relationship between these parameters and the PSD are given in the following:

[21] The normalization parameter:

$$N_0^* = \frac{4^4}{6}\frac{\left(\int N(D_{eq})D_{eq}^3 dD_{eq}\right)^5}{\left(\int N(D_{eq})D_{eq}^4 dD_{eq}\right)^4} m^{-4} \tag{16}$$

[22] The effective radius [*Stephens et al.*, 1990]:

$$r_e = \frac{1}{2}\frac{\int N(D_{eq})D_{eq}^3 dD_{eq}}{\int N(D_{eq})D_{eq}^2 dD_{eq}} \text{ in m} \tag{17}$$

Several definitions of this parameter are proposed in the literature, since effective radius cannot be as clearly defined in the case of ice clouds as it is in the case of liquid drops, owing in particular to large asphericities of ice crystals. We have chosen to use the definition proposed by *Stephens et al.* [1990], which has the advantage of being expressed in terms of the equivalent melted diameter as in our study. It is noteworthy however that this definition does not accurately describe the effects due to the cross-sectional area of the particles. More elaborated expressions have been proposed in the literature [e.g., *McFarquhar and Heymsfield*, 1998], but these formulations rely on the cross-sectional area and its relation to the maximum crystal diameter, which is generally not available in our database. This is not very critical, however, since the purpose of this study is not to study the quantitative values of effective radius itself, but the errors on this parameter arising from the assumption of an universal shape for the normalized ice PSD.

[23] The equivalent radar reflectivity Z_e: At 3 GHz where the refractive index of water depends only slowly with temperature, the radar reflectivity Z due to the particle spectrum is defined as

$$Z = \int N(D)D^6 dD \tag{18}$$

and may be related without ambiguity to the power of the backscattered signal. At 94 GHz, the refractive index of water varies rapidly with temperature, thus it is convenient at these high frequencies (and this is what is generally done in radar-meteorology) to refer to the equivalent reflectivity that would be observed at 3 GHz. Moreover, the ice particles have a quite different refractive index from water, and their size is such that we may get into the Mie scattering regime. Thus it is convenient to define an equivalent radar reflectivity Z_e, comparable to the 3 GHz frequency, and unambiguously related to the power of backscattered signal. The equivalent radar reflectivity in the Mie regime can be written as:

$$Z_e = \frac{\lambda^4}{|K_w|^2\pi^5}10^{18}\int N(D_{eq})\sigma_{bsc}dD_{eq} \text{ mm}^6.\text{m}^{-3} \tag{19}$$

where σ_{bsc} is the backscattering cross section.

[24] In the Rayleigh approximation when $D < 0.08\ \lambda$,

$$Z_e = \frac{|K_i|^2}{|K_w|^2}\left(\frac{\rho_w}{\rho_i}\right)^2 10^{18}\int N(D_{eq})D_{eq}{}^6 dD_{eq} \qquad (20)$$

with $|K_i|^2 = 0.176$ at 94 GHz and $|K_w|^2 = 0.93$ at 3 GHz.

[25] The reflectivity weighted velocity

$$V_{tz} = \frac{\int v(D_{eq})\sigma_{bsc}N(D_{eq})dD_{eq}}{\int \sigma_{bsc}N(D_{eq})dD_{eq}}\ \mathrm{m.s^{-1}} \qquad (21)$$

In the same way as for density, a velocity-diameter relationship must be assumed to compute the reflectivity-weighted terminal fall velocity. In the following the velocity-diameter model of *Mitchell* [1996] has been used, and spherical aggregates have been considered, in order to remain consistent with the Locatelli and Hobbs density-diameter relationship assumed for the other calculations. It is to be noted that the dependency of the velocity-diameter relationship on the atmospheric pressure has also been accounted for in the calculation. The sensitivity of the results presented in this study to the v(D) relationship will be conducted at the same time as the sensitivity analysis for density.

[26] Extinction and specific attenuation:

$$\alpha = 2.10^3 \int N(D)A(D)dD\ \mathrm{km^{-1}} \qquad (22)$$

where A(D) is the cross-sectional area/diameter relationship. Again, the sensitivity of the results presented in this paper to the A(D) relationship will be evaluated in section 4.

$$K = 4.34294.10^3 \int N(D_{eq})\sigma_{abs}dD_{eq}\ \ \mathrm{dB.km^{-1}} \qquad (23)$$

where σ_{abs} is the absorption coefficient.

3. Database Presentation

[27] The purpose of this study is to work out the stability in shape of the normalized PSD in ice clouds, and to study the variability of the two parameters of the PSD, D_m and N_0^*. The main question here is: are the statistical properties of the normalized ice cloud PSD independent of temperature, type of ice cloud, and geographical location (midlatitude versus tropics)? For these reasons a large statistical microphysical database has been first gathered, which is described in the following, including midlatitude and tropical field campaigns:

3.1. Methodology

[28] The particle size distribution N(D) is provided by airborne PMS (Particle Measuring Systems) 2D-C (2D Cloud) and 2D-P (2D Precipitation) microphysical probes. 2D-C and 2D-P probes belong to the Optical Array Probes. Shadow images of cloud particles are in size ranges between 25 and 800 μm for the 2D-C and between 200 and 6400 μm for the 2D-P, with diameter intervals of 25 and 200 μm, respectively.

[29] Recent field campaigns also include Forward Scattering Spectrometer Probe (FSSP) data, but not all of the experiments in the database do. Therefore we have chosen not to use the FSSP data, in order to keep the different field experiments comparable.

[30] A common difficulty with all of these sensors is due to the small collection area of the instrument, which makes the particle counting in each diameter class very noisy, especially for large particle, which have the smallest concentration. These individual samples are therefore averaged over a given time period in order to reduce noise.

3.2. Data Description

3.2.1. Midlatitude Experiments

[31] CLARE98: The Cloud Lidar And Radar Experiment took place from 5 to 23 October 1998 at the Observatory of Chilbolton, Hampshire, UK. This campaign was devoted to the characterization of the microphysical, radiative and dynamic properties of nonprecipitating clouds. For this purpose a ground-based combination of cloud radar, lidar and radiometers has been deployed, as well as airborne instrumentation including an in situ microphysics aircraft and an active remote sensing aircraft. The UK C-130 was performing the in situ microphysical documentation of the clouds using the FSSP, 2D-C and 2D-P probes. In this data set, we considered 9 legs over two days, 3 flights on 14th October and 6 flights on 20th October, which corresponds to 1h24 of ice cloud data have been extracted for our analysis with an integration time about 5s.

[32] CARL99: The investigation of Cloud by Ground-based and Airborne Radar and Lidar campaign was held in Palaiseau (France) in April–May 1999. This campaign was devoted to the investigation of the ice cloud properties and involved ground-based lidar, radar and radiometry measurements as well as in situ validation measurements from aircraft. The Merlin IV aircraft from Météo-France was carrying the set of in situ microphysical probes from GKSS (FSSP, 2D-C and 2D-P). This data set corresponds to 2h10 (integration time 10s) of data in our analysis, over two days: the 29th April and 4th May 1999.

[33] ARM (Atmospheric Radiation Measurement Program) Intensive airborne microphysical observations above the ARM Southern Great Plains (SGP) instrumented site have been carried out in 2000. The scientific objectives of these flights were to improve cloud and radiative models and parameterizations and, thereby, the performance of atmospheric general circulation models used for climate research. Four days of March 2000, including Lagrangian spirals descents, are in our database. This corresponds to 15h35 of observations (1s resolution).

[34] EUCREX (European Cloud Radiation Experiment) was a program focused on the Earth radiation budget and climate change, starting in 1991 through 1995. A principal aim of EUCREX was to improve our knowledge of the physical processes that determine the radiative transfer properties of cloud fields. Primary attention was given to cirrus clouds, with the study of stratiform cloud fields as a secondary aim. Eucrex'93 took place off the Scottish coast. Airborne in situ microphysical measurements were collected using the 2D-C and 2D-P probes onboard the U.K.

Table 1. Flights Hours and Integration Time in Our Analysis

Experiments	Data Hours	Integration Time, s
CLARE98	1h24	5
CARL99	2h10	10
EUCREX	20h25	5
FASTEX	83h	10
ARM	15h35	1
CEPEX	35h	10
CRYSTAL FACE	41h	5

C-130 research aircraft. The sampled cirrus clouds were generally thick and frontal in origin. In our analysis, data sets comprises a total of 14704 5s averaged size spectra measured at temperatures between −10 and −50°C.

[35] FASTEX (Fronts and Atlantic Storm-Track Experiment) took place in January–February 1997 off the Irish Coast over the North Atlantic. This international campaign was in part devoted to the study of multiscale processes associated to the mature stage of frontal cyclogenesis. 10 flights of the UK-C130 aircraft instrumented with the 2D-C sensors have been performed in the ice part of frontal cyclones, corresponding to 83 hours of data in our analysis, with an integration time around 10s.

3.2.2. Tropical Experiments

[36] CEPEX (Central Equatorial Pacific Experiment) was conducted between 7th March and 5th April 1993 within the geographical area bounded by 20°S to 2°N and 165°E to 170°W. Of the 108 flight hours logged by the Learjet aircraft during CEPEX, three flights including 2D-C and 2P-P probes were designed to measure the vertical and horizontal structure of cirrus microphysical properties. The CEPEX data set sampled tropical ice clouds, with 12500 10s averaged size spectra with temperatures between −65°C and −10°C.

[37] CRYSTAL-FACE (Cirrus Regional Study of Tropical Anvils and Cirrus Layers - Florida Area Cirrus Experiment) is a measurement campaign designed to investigate tropical cirrus cloud physical properties and formation processes. It took place in July 2002 around Florida. Several aircraft were involved for in situ and remote sensing of ice crystals. Among these aircraft the Cessna Citation II aircraft of the University of North Dakota, carried a state-of-the-art set of in situ microphysical instruments: 2D-C probes, Continuous Flow Diffusion Chamber (CFDC), Cloud Integrating Nephelometer (CNI), Cloud Particle Imager (CPI) and High Volume Precipitation Spectrometer (HVPS), but not the 2D-P probe used in our analysis for all the other experiments. Spectra used in our study have therefore been constructed using a combination of the 2D-C and HVPS. This data set corresponds to 41 hours with a 5s integration time. All flights hours and integration times are summarized in Table 1.

4. Statistical Study of the Normalized Ice PSD Shape

4.1. Is the Normalized PSD Shape as Stable as the Raindrop Size Distribution?

[38] As briefly reviewed in the previous section, the radar and lidar observables, as well as the microphysical and radiative properties of clouds can be computed from the PSD. As a result, any forward model between radar/lidar observables and cloud properties includes the statistical properties of the PSD. It is therefore important to investigate the statistical properties of the shape and parameters that characterize the PSD of ice clouds. Any simplification of the problem would result in a reduction of the number of observations required to access the cloud properties when inverting the forward model. In this section we will first investigate the stability of the shape of the PSD in ice clouds using the extensive database cited earlier.

[39] From each component of the observed spectrum N (D_i), the corresponding component of the normalized spectrum F (X_i) = N (D_{eqi})/N_0^*, where $X_i = D_{eqi}/D_m$ was calculated. We have then considered classes in normalized diameter X with width of 0.1 and calculated the mean value of F(X). In order to compare the normalized PSD of all experiments we have then computed a single mean PSD, which is obviously not as noisy as the individual normalized spectra. The density of points has however been displayed as grey-level contours in order to keep track of the PSD variability. It is to be noted that we did not use the error-bar type of display of the variability of the spectra, owing to the fact that in logarithmic scale the standard deviation increases sharply and when $\sigma/\overline{F}(X)$ reaches 1, the lower bound of the error bar goes to infinity.

[40] The mean normalized PSD shape (i.e., $N(D_{eq}/D_m)/N_0^*$ as a function of D_{eq}/D_m) and density contours derived from each airborne in situ microphysical experiment CLARE98, CARL 99, EUCREX, FASTEX, ARM, CEPEX, and CRYSTAL-FACE are displayed in Figure 1, as well as the amount of measurements in each class of normalized diameter. It is to be noted that we have retained the empty classes as relevant information in the average. The mean normalized PSD including all the experiments is shown for comparison in Figure 2. Also shown in each panel of Figures 1 and 2 are three analytical shapes for reference: the exponential shape, the gamma-μ shape (with $\mu = 3$), and the modified gamma shape with $(\alpha, \beta) = (-1, 3)$.

[41] It is clearly seen from Figures 1 and 2 that most measurements are concentrated between $D_{eq}/D_m = 0$ and 2, with very little scatter around the mean (see grey contours) for all experiments. This area corresponding to $D_{eq}/D_m < 2$ is fairly invariant from an experiment to another, while the "tail" of the PSD (i.e., the part of the plots corresponding to $D_{eq}/D_m > 2$) is much more variable. In some experiments (CLARE98, EUCREX, CRYSTAL-FACE) this tail is indeed close to exponentiality, as is the case of stratiform rain, while for the others this tail is better described by the gamma μ shape. It will be shown however in the next section that the sensitivity of the cloud properties to the variability of the PSD tail is small, owing to the much larger concentration of ice particles in the range $D_{eq}/D_m = [0,2]$ shown in Figures 1 and 2.

[42] A closer inspection of Figure 1 shows a systematic difference between the midlatitude and the tropical experiments in this range of small D_{eq}/D_m. For the tropical experiments (CEPEX and CRYSTAL-FACE) the normalised PSD is very stable and the tail variability is smaller for $D_{eq}/D_m < 3$ than for the midlatitude experiments (Figure 3). The majority of points is again concentrated between $D_{eq}/D_m = 0$ and 2 and the exponential shape seems to be an excellent approximation for the tropical ice cloud PSDs

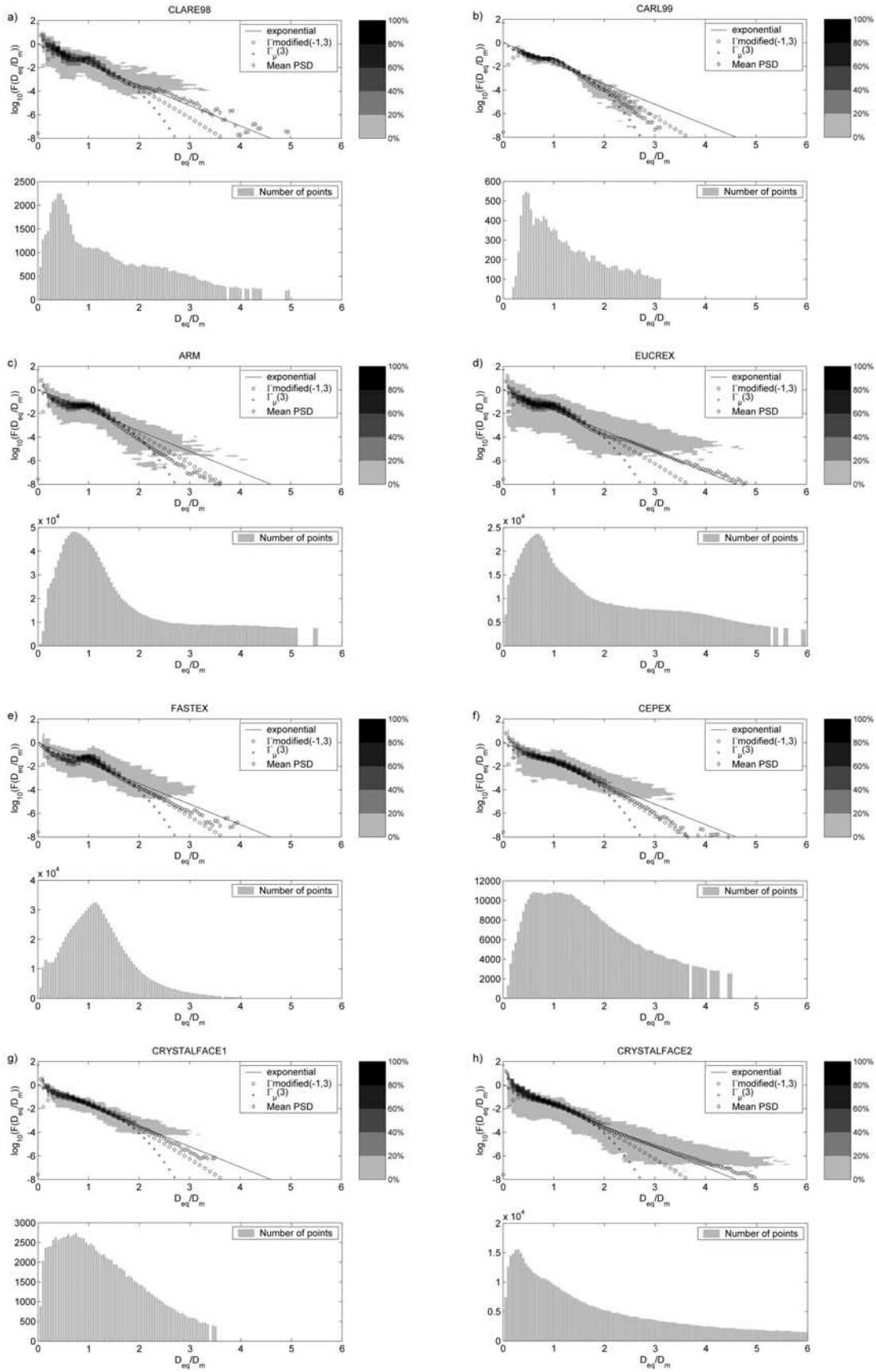

Figure 1. Normalized particle size distribution for each experiment ((a) CLARE98, (b) CARL99, (c) ARM, (d) EUCREX, (e) FASTEX, (f) CEPEX, (g) CRYSTAL-FACE1, and (h) CRYSTAL-FACE2).

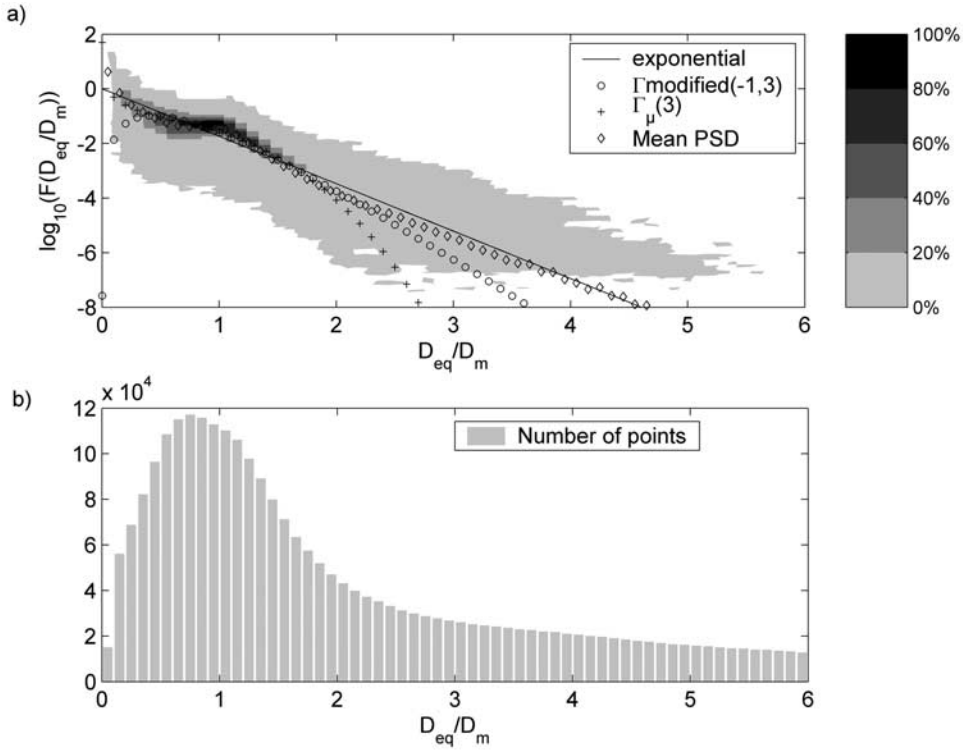

Figure 2. (a) Contour density of normalized PSD from all spectra of the data set. Also displayed for reference are the analytical shapes discussed in the text: modified gamma with couple coefficients (−1, 3), gamma $\mu = 3$, and exponential. (b) Number of points.

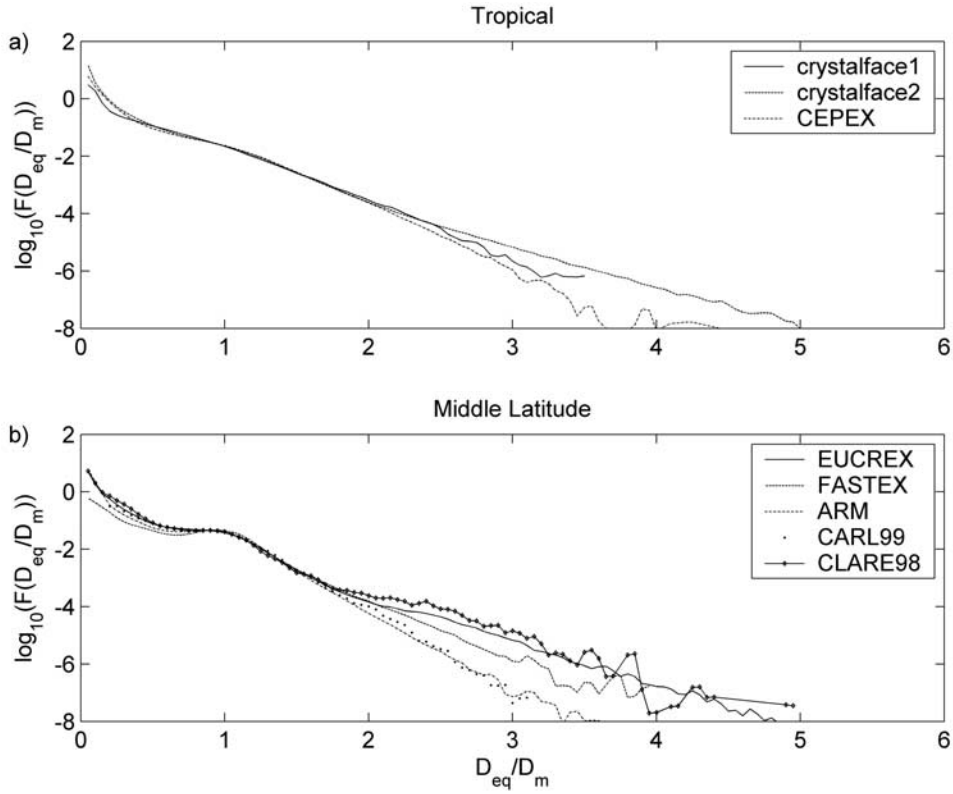

Figure 3. Mean normalized PSDs of (a) the tropical experiments (CEPEX, CRYSTAL-FACE), and (b) the midlatitude experiments (EUCREX, FASTEX, ARM, CARL99, CLARE98).

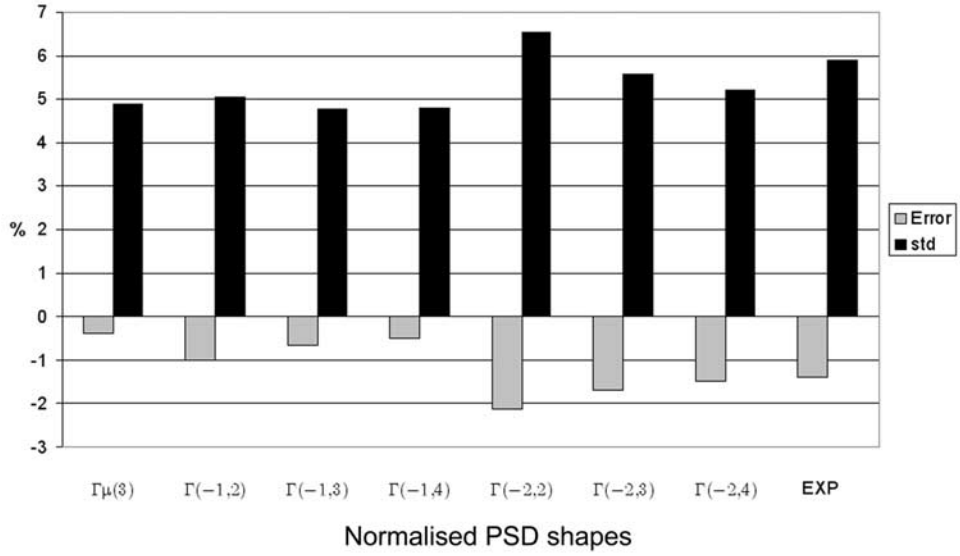

Figure 4. Mean relative error including all instrumental and cloud parameters as a function of the following analytical PSD shapes: exponential, gamma with $\mu = 3$ and different modified gamma shapes (see text).

in this range. Regarding the midlatitude experiments (CLARE98, CARL99, EUCREX, ARM and FASTEX) the mean PSDs all exhibit a bow-shaped structure with a bump centred on $D_{eq}/D_m = 1$. If the objective is to represent these midlatitude PSDs with a single analytical shape, it is clear from Figure 1 that this bump is best fitted by the gamma ($\mu = 3$) and modified gamma (-1, 3) analytical shapes. This will be evaluated in further detail in the next section. In the case of raindrop size distribution this bump has also been observed by TAL01, who attributed it physically to the *Hu and Srivastava* [1995] concept of "equilibrium" drop size distribution, which reflects the growth of raindrops up to an equilibrium size, corresponding to a given rainfall. This main difference between midlatitude and tropical regions can be interpreted as a natural trend in the Tropics to have a wider distribution of particle diameters around the volume weighted diameter D_m, which seems to be much narrower at midlatitudes. This could be attributed to different growth processes of ice particles involved in different precipitating systems (long-lasting frontal systems at midlatitudes versus intense mesoscale convective systems in the Tropics). This hypothesis could certainly be investigated with high-resolution numerical cloud modelling, which is beyond the scope of this paper and the skills of this research team.

[43] Globally we can therefore consider from this analysis that the normalized PSD shape is reasonably stable in ice clouds, with a remarkable stability of the mean PSD for normalized particle diameters smaller than 2, and a larger variability of the PSD tail. In the next section we perform an analysis of the errors associated with the use of four different analytical PSD shapes for all midlatitude and tropical ice clouds.

4.2. Can We Use a Single Analytical PSD Shape for Ice Clouds?

4.2.1. Global Error Analysis

[44] Three analytical formulations of the PSD shape, which have been described in section 2, are used in the present section to develop a single analytical PSD shape for ice clouds. The error analysis consists of a computation of the mean error and standard deviation of the difference between (1) the "true" instrumental parameters (that is, the radar reflectivity Z_e, radar attenuation K) and ice cloud properties (ice water content IWC, effective radius r_e, terminal fall velocity of ice crystals Vt_Z, lidar extinction α) calculated using the individual in situ spectra from all the experiments, and (2) the same instrumental parameters and cloud properties calculated from the "true" in situ (N_0^*, D_m) and each analytical PSD shape. Following this procedure, the individual impact of using a single analytical shape is directly obtained. As discussed previously, calculations are first done in this section using the *Locatelli and Hobbs* [1974] density-diameter relationship, and the fall velocity for spherical aggregates using the *Mitchell* [1996] formulation. Then in section 4.2.4 we will analyse the sensitivity of the results presented in this section to the particle type, characterized by its corresponding $\rho(D)$, $v(D)$, and $A(D)$ relationships.

[45] The following analytical shapes have been used: (1) The exponential shape (9). (2) The $\Gamma_{\mu=3}$ shape (11). The value $\mu = 3$ has been obtained by minimizing in the least-squares sense the difference between the mean PSD of Figure 2 and the gamma μ expression (11). (3) The modified gamma shapes (13), with the following (a,b): $\Gamma_m(-1, 2)$, $\Gamma_m(-1, 3)$, $\Gamma_m(-1, 4)$, $\Gamma_m(-2, 2)$, $\Gamma_m(-2, 3)$, $\Gamma_m(-2, 4)$.

[46] Let us first analyze the mean error on all parameters and for all experiments in order to extract the most relevant shapes for a further error analysis. This global error analysis is summarized in Figure 4, showing the mean relative error (grey bars) and standard deviation (black bars) on all parameters for the different analytical shapes. Overall, there is not much difference between the analytical shapes, with a bias that doesn't exceed 2% and a standard deviation less than 7%. The most accurate shapes are the $\Gamma_{\mu=3}$, the $\Gamma_m(-1, 4)$ and the $\Gamma_m(-1, 3)$, with biases of -0.4%, -0.5% and -0.66%, and standard deviations of 4.9%, 4.8% and

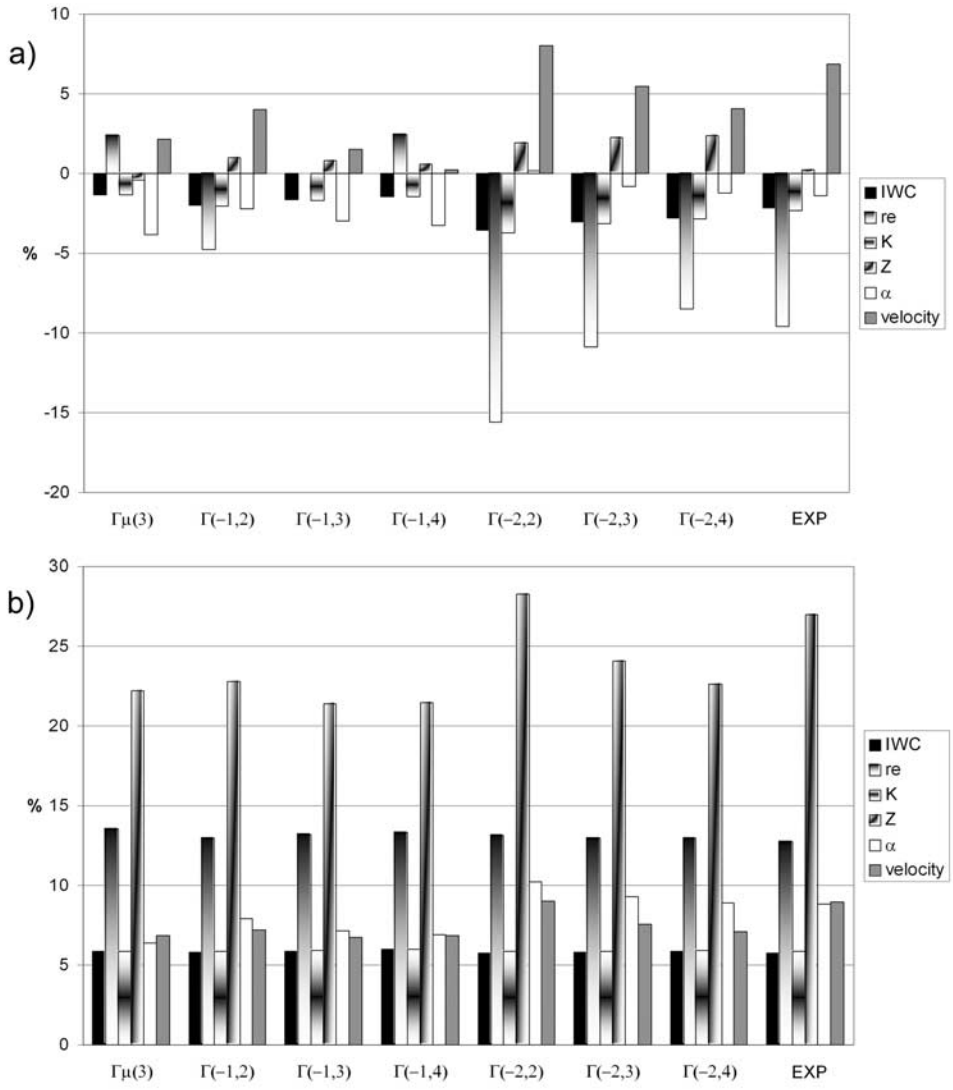

Figure 5. (a) Mean relative error and (b) standard deviation on IWC, r_e, Z, V_{tZ}, α, and K as a function of the following analytical PSD shapes: exponential, gamma with $\mu = 3$ and different modified gamma shapes (see text).

4.75%, respectively. This global result is confirmed by Figure 5, which shows the individual mean error (upper panel) and standard deviation (lower panel) for each parameter IWC, Z_e, α, K, r_e, Vt_Z as a function of the analytical shape. The mean relative error on each parameter is clearly minimized when using the $\Gamma(-1, 4)$, $\Gamma(-1, 3)$ and $\Gamma_{\mu=3}$ shapes, leading to biases of less than 3% for all parameters. The standard deviations on all the parameters is roughly comparable for all shapes, except for α and Vt_Z for which the $\Gamma(-1, 4)$, $\Gamma(-1, 3)$ and $\Gamma_{\mu=3}$ shapes produce smaller standard deviations. All analytical shapes seem to produce stronger standard deviations on Z_e than for the other parameters. It must be noted however that this error on reflectivity in mm^6m^{-3} reduces to less than a dB in logarithmic scale, which is smaller than the calibration accuracy generally attainable. It is also seen that the exponential shape, which is widely used in the literature, does well for the mean errors on IWC, K, Z_e, and α (mean error less than 3%, and standard deviations roughly comparable to the good analytical shapes), not that well for r_e and Vt_Z (larger biases of around −10% and 7% for r_e and Vt_Z, respectively).

[47] In conclusion, the $\Gamma(-1, 4)$, $\Gamma(-1, 3)$ and $\Gamma_{\mu=3}$ shapes can be used as an accurate approximation for any ice particle size distribution, and for any instrumental or cloud parameter to be derived from the PSD. If the exponential shape is to be used, it is fairly accurate for IWC, K, Z_e, and α, and slightly less accurate for r_e and Vt_Z.

4.2.2. Error Analysis as a Function of Temperature

[48] In what follows, the exponential, $\Gamma(-1, 4)$, $\Gamma(-1, 3)$ and $\Gamma_{\mu=3}$ analytical shapes are retained in order to describe the distribution of these errors as a function of temperature. For this purpose, we have computed the mean error and standard deviation in 10°C temperature intervals. Figure 6 shows the histogram of the amount of measurements in each 10°C temperature interval. The vast majority of points is concentrated in the interval [−50°C, −10°C], for which it can be considered that the error estimate is most statistically significant.

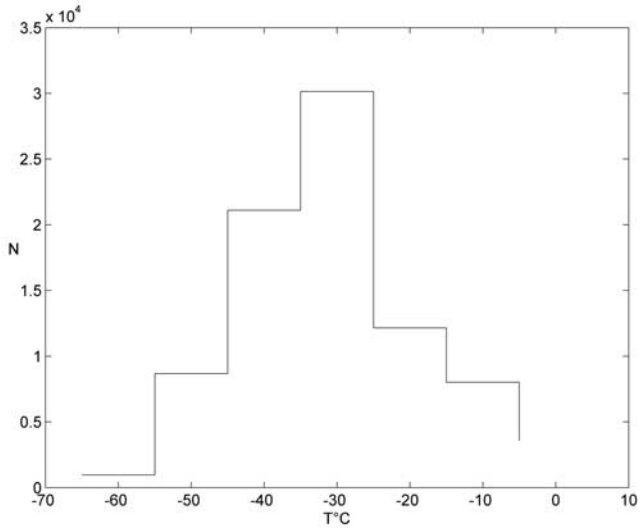

Figure 6. Amount of points used to compute the mean error in each temperature interval.

[49] The Ice Water Content (IWC) and specific radar attenuation K: Figures 7–10 show the mean relative error on IWC and K as a function of temperature, when the four analytical shapes are used. From −65°C to −35°C, the mean error of the two parameters is similar. It is found to be very small (less than 2%), and it tends to increase up to around −5% at −20°C/−10°C. The standard deviation is very stable and near 5–6% for all shapes. This analysis shows that all shapes can produce an accurate estimate of IWC and K at any temperature.

[50] The effective radius (r_e): As illustrated in Figures 7–10 for the different shapes, if we consider the temperature between −50 and −10°C the standard deviation of the relative error doesn't exceed 14% for all shapes and does not change much as a function of temperature. The use of the exponential shape yields a bias that increases with temperature from 0% to −16% in the [−55°C, −35°C] range, and decreases down to 0% at −10°C. The trend is the opposite for the $\Gamma\mu = 3$, $\Gamma_m(-1, 3)$ and $\Gamma_m(-1, 4)$ analytical shapes, with a decrease of the bias from around 12% to 0% in the [−65°C, −35°C] range, and an increase from 0% to 20% in the [−35°C, −10°C] range. Therefore the use of any of the $\Gamma_{\mu=3}$, $\Gamma_m(-1,3)$ and $\Gamma_m(-1,4)$ analytical shapes result in an absolute bias less than 5% and a standard deviation of around 12–14% in the [−50°C, −15°C] range.

[51] The radar reflectivity factor Z_e (Mie): The mean relative error on Z_e ranges from +15% when $-65 < T < -40$°C to −15% within the [−40; −10°C] temperature range. In the case of the gamma shapes the bias is less than 4% in the interval [−50, −20°C]. The standard deviation is around 20% for the gammas and 25% for the exponential. Again, this does not represent a large error (<1 dB), smaller than the foreseen calibration error of radars.

[52] The visible extinction: The standard deviation and mean error are roughly the same for all shapes (around 6–8% and −4%, respectively) and do not vary significantly with temperature. All shapes are therefore able to produce a fairly accurate estimate of the visible extinction.

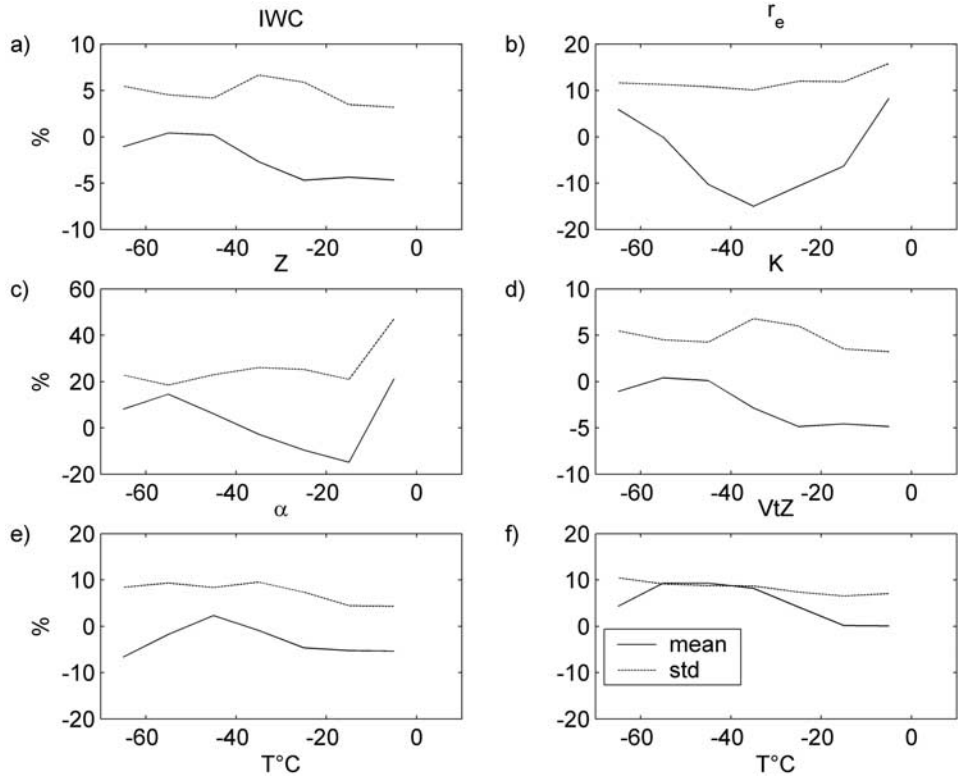

Figure 7. Mean relative error and standard deviation on (a) IWC, (b) r_e, (c) Z, (d) K, (e) α, and (f) V_{tZ} as a function of temperature for the exponential shape.

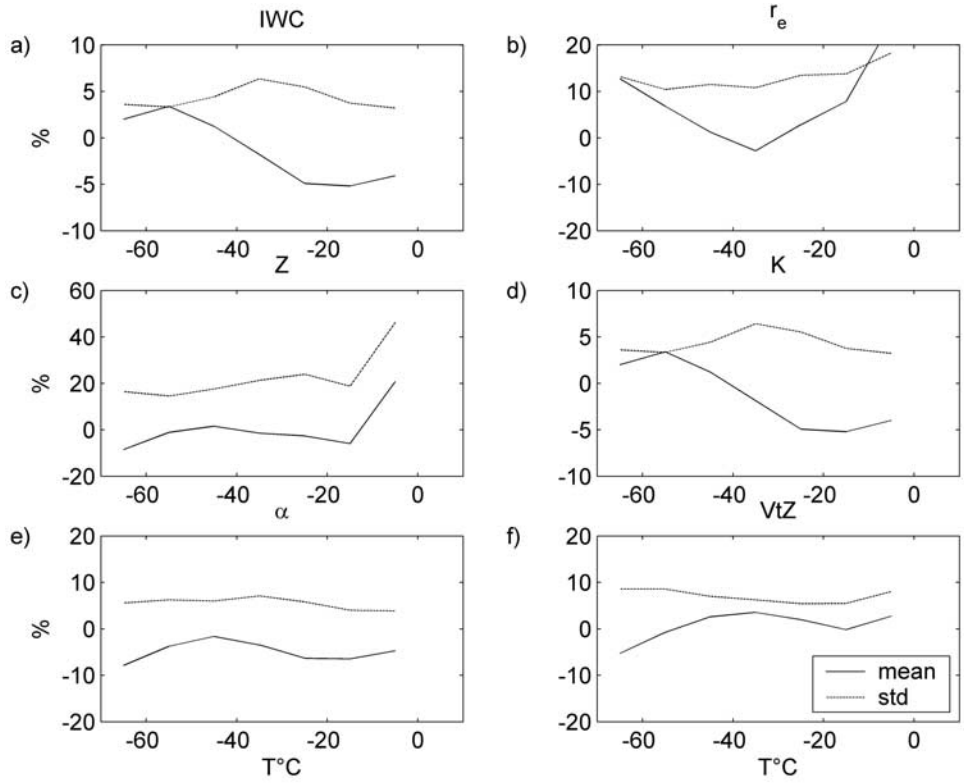

Figure 8. Same as Figure 7, but for the gamma $\mu = 3$ shape.

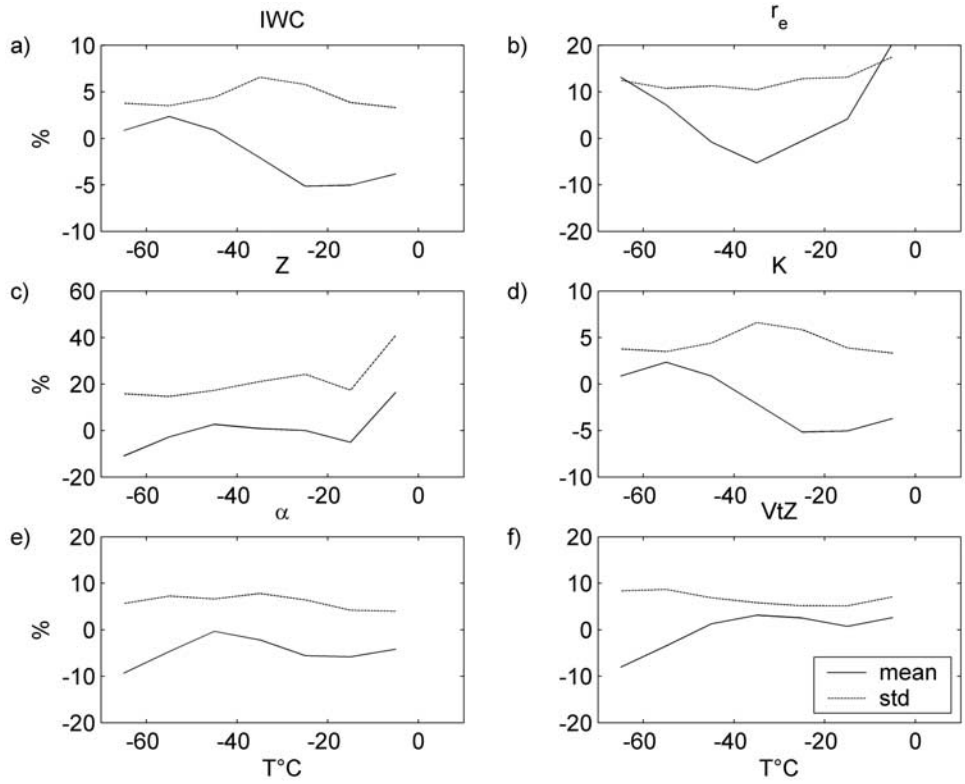

Figure 9. Same as Figure 7, but for the modified gamma(−1, 3) shape.

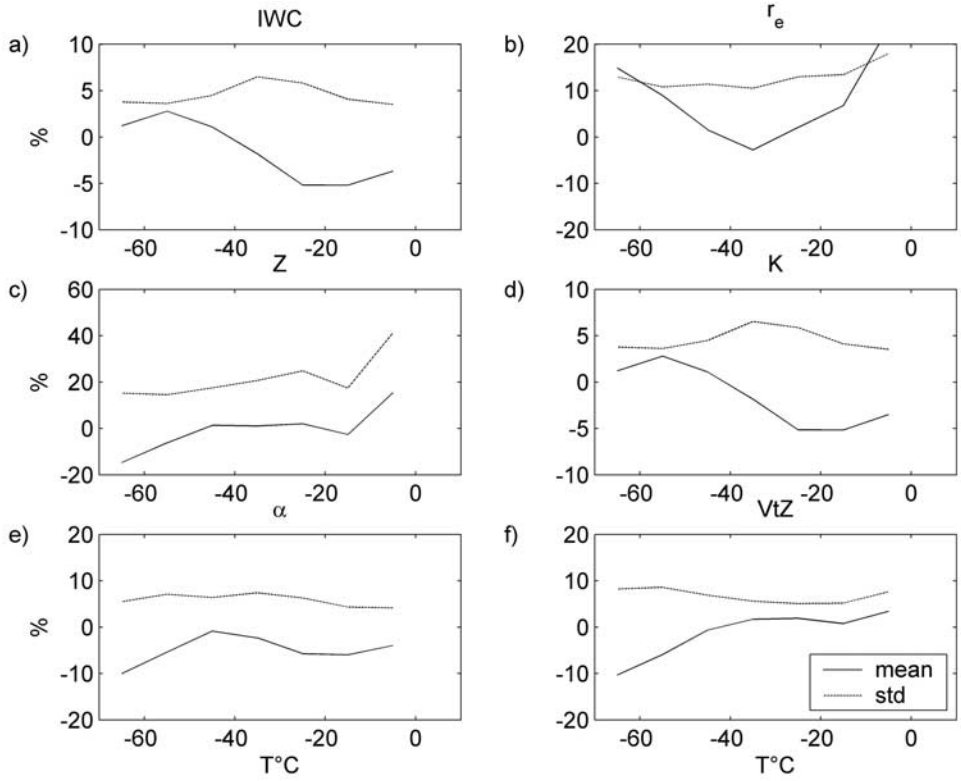

Figure 10. Same as Figure 7, but for the modified gamma(−1, 4) shape.

[53] The reflectivity-weighted velocity: The standard deviation is around 10% for the exponential shape and 8% for all gamma shapes and relatively constant in the whole temperature range. The mean error is however larger with the exponential shape for all temperatures (around 8–10%) than for the modified gamma shapes (around −8% for the lowest temperatures, but less than 5% for temperatures greater than −50°C). The best estimate is achieved with the $\Gamma_{\mu=3}$, with absolute mean errors less than 4% at all temperatures.

4.2.3. A Possible Refinement for Tropical PSDs Versus Midlatitude PSDs

[54] In the previous section it has been shown that the cloud parameters derived from the gamma distributions were in general more accurately determined than with the exponential shape. However, as seen in Figure 1, the tropical ice normalized PSDs seem to be closer to exponentiality, owing to a spread of diameter values around the mean volume-weighted diameter larger than at midlatitudes, which results in a much less marked bump for tropical PSDs around $D_{eq}/D_m = 1$, as discussed previously. This difference may be attributed to the fact that midlatitude ice clouds are generally produced by a large scale uplift while tropical ice clouds are rather triggered by convection. In this section we have therefore split the midlatitude and tropical experiments and conducted an error analysis similar to that of Figure 5, which is presented in Figure 11 for the tropical experiments. From this separate analysis it appears that the $\Gamma_{\mu=3}$, $\Gamma_m(-1, 3)$ and $\Gamma_m(-1, 4)$ analytical shapes are still the most accurate for midlatitude ice PSDs (not shown). However, it is clearly seen in Figure 11 that the exponential shape produces a much smaller mean error for effective radius and a slightly smaller mean error for extinction in the Tropics, but a larger mean error for the other parameters. Other tests (not shown) indicate that a $\Gamma_m(-2, 3)$ analytical shape, which is characterized by a less-marked bump, also results in an unbiased estimate of effective radius. The standard deviations are roughly similar for all shapes.

4.2.4. Density and Velocity Diameter Relationships Impacts on the Precedent Results

[55] As previously mentioned in section 2.3.1 the choice of a density-diameter, velocity-diameter, and cross-sectional area/diameter relationship related to an assumed particle type could potentially alter the results obtained up to now in this study, which are the fair stability of the normalized PSD shape, and the possible use of a single analytical shape to represent this shape for all ice clouds. In order to investigate how these results are altered by this assumption, we have considered two additional particle types that can be thought of as spanning the natural variability encountered in ice clouds: hexagonal columns and hexagonal plates. The formulations of ρ(D), v(D), and A(D) relationships for these two particle types are those from *Mitchell* [1996].

[56] From these new relationships the same procedure as that presented in section (4.2.1) has been followed. We have again considered three normalized PSD shapes: exponential, $\Gamma_{\mu=3}$, and $\Gamma_m(-1, 3)$, and computed the mean error and standard deviation of the difference between the "true" instrumental parameters and ice cloud properties calculated using the individual in situ spectra from all the experiments, and the same instrumental parameters and cloud properties calculated from the "true" in situ (N_0^*, D_m) and each analytical PSD shape.

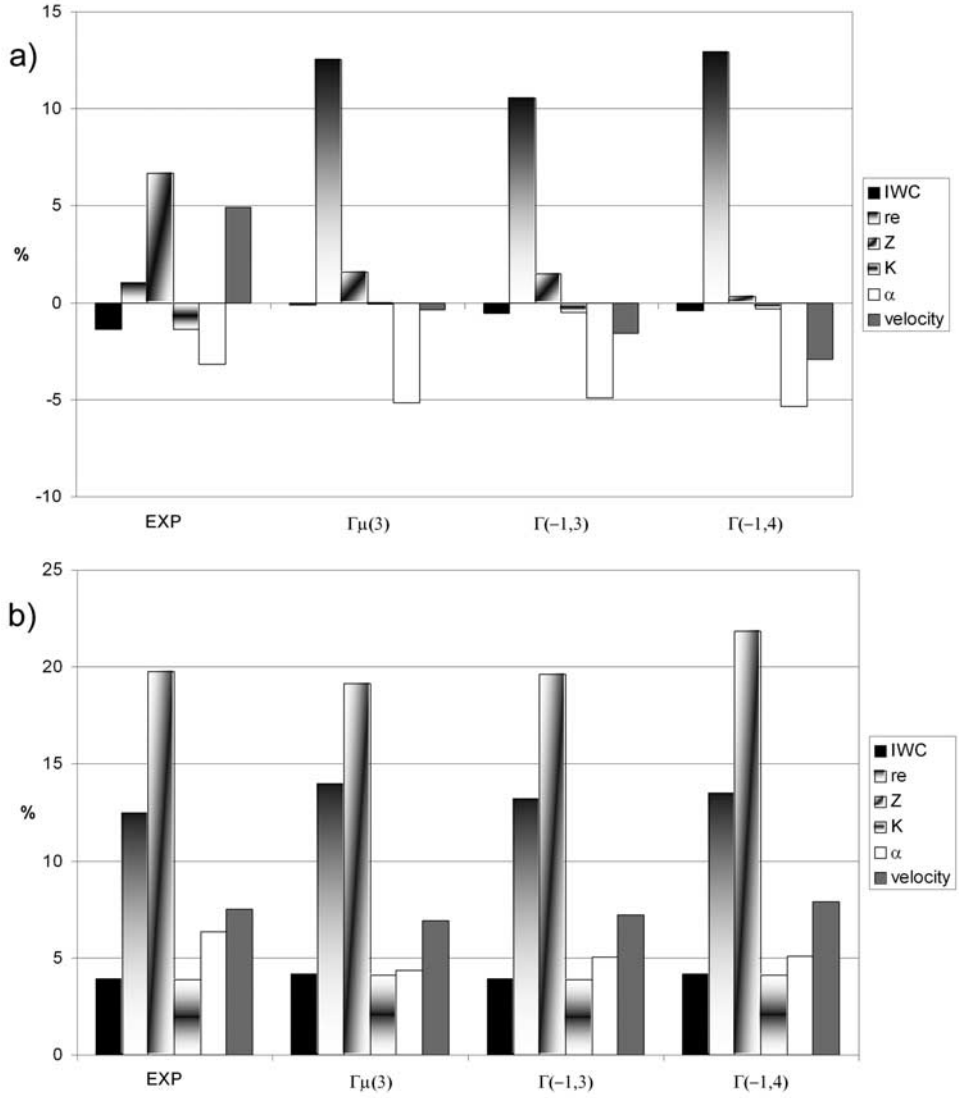

Figure 11. Same as Figure 5, but for the tropical experiments only.

[57] As shown in Figures 12 and 13, the best results are still obtained by the modified gamma (−1, 3) for the two sets of particle types, with about the same mean errors and standard deviations as those found when the *Locatelli and Hobbs* [1974] relationships are used. This result shows that the conclusions on the normalized PSD shape presented up to now are not altered by the assumption on particle type.

5. Statistical Study of the N_0^* and D_m Parameters of the Normalized Ice PSD Shape

[58] In section 4, we have demonstrated the stability of the PSD shape and showed that it was possible to represent the shape of the normalized ice PSDs by a single analytical formulation, which in addition does not depend on the particle type. This stability in shape (and its unique analytical approximation) implies that two parameters are now sufficient to describe any normalized PSD of ice clouds: N_0^* and D_m. In this section, we investigate different possibilities to reduce again the number of unknowns by developing and evaluating statistical relationships (parameterizations) between N_0^* and D_m.

5.1. Parameterization of N_0^* and D_m With Temperature

[59] We have first investigated the potential of simple relationships between each parameter and temperature. Let us recall that many large-scale model parameterizations diagnose an ice particle diameter from a mean maximum diameter – temperature relationship [e.g., *Kristjánsson et al.*, 2000]. Figure 14 shows the scatterplots of N_0^* and D_m as a function of temperature. A clear trend is obtained for both plots: $\log_{10}(N_0^*)$ decreases and D_m increases when temperature increases. This trend is qualitatively consistent with the fact that colder temperatures are usually associated with a large number of small particles, while the aggregation process in ice clouds tends to produce larger ice particles in smaller amounts as ice crystals fall (corresponding to higher temperatures). The scatter around the mean fits to the data is however very large, and this scatter is not reduced when splitting into tropical and

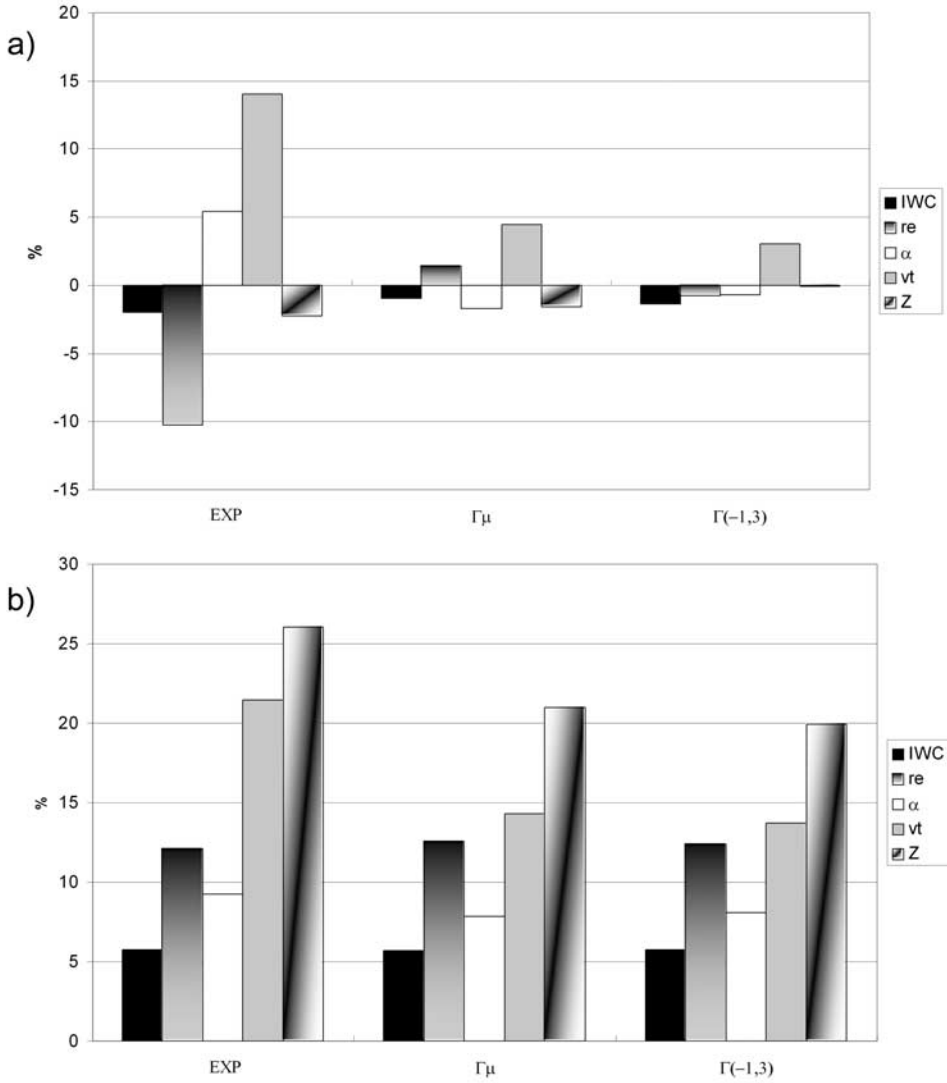

Figure 12. Assuming *Mitchell* [1996] hexagonal columns ice particle: (a) Mean relative error and (b) standard deviation on IWC, r_e, Z, V_t, α as a function of the following analytical PSD shapes: exponential, gamma with $\mu = 3$, and modified gamma shape.

midlatitude experiments (not shown). Two error analyses on the instrumental and cloud parameters have therefore been conducted in order to study the potential of using such parameterizations:

[60] Errors using the true D_m and the N_0^*-T parameterization of Figure 14: This parameterization produces very large mean errors and standard deviation of the mean errors (not shown), owing to the huge standard deviation of N_0^* for a given temperature (several orders of magnitude). Therefore this parameterization cannot be retained here for any application.

[61] Errors using the true N_0^* and the D_m -T parameterization of Figure 14: An exponential function has been fitted to the data, as had been done in earlier studies to parameterize D_m in climate models. We have obtained the following relationship for the Locatelli and Hobbs density/diameter relationship:

$$D_m = 0.4002 \exp[0.029(T + 253.3)] \quad (24)$$

with T in °C and D_m in μm.

[62] Since D_m is defined as the ratio of the fourth to the third moment of the PSD in D_{eq}, D_m depends on the particle type. For this reason we extend the study to the two other density/diameter relationships used in the section (4.2.4) which are believed to span the range of possible densities encountered in ice clouds: Hexagonal columns:

$$D_m = 274.355 \exp[0.0255(T + 17.2)] \quad (25)$$

Hexagonal plates:

$$D_m = 8.327 \exp[0.0418(T + 110)] \quad (26)$$

These three D_m-T relationships are plotted in Figure 15. From this figure it appears that the D_m-T relationship is not very variable in the [−70°C; −30°C] temperature range while it gets very sensitive to the density diameter

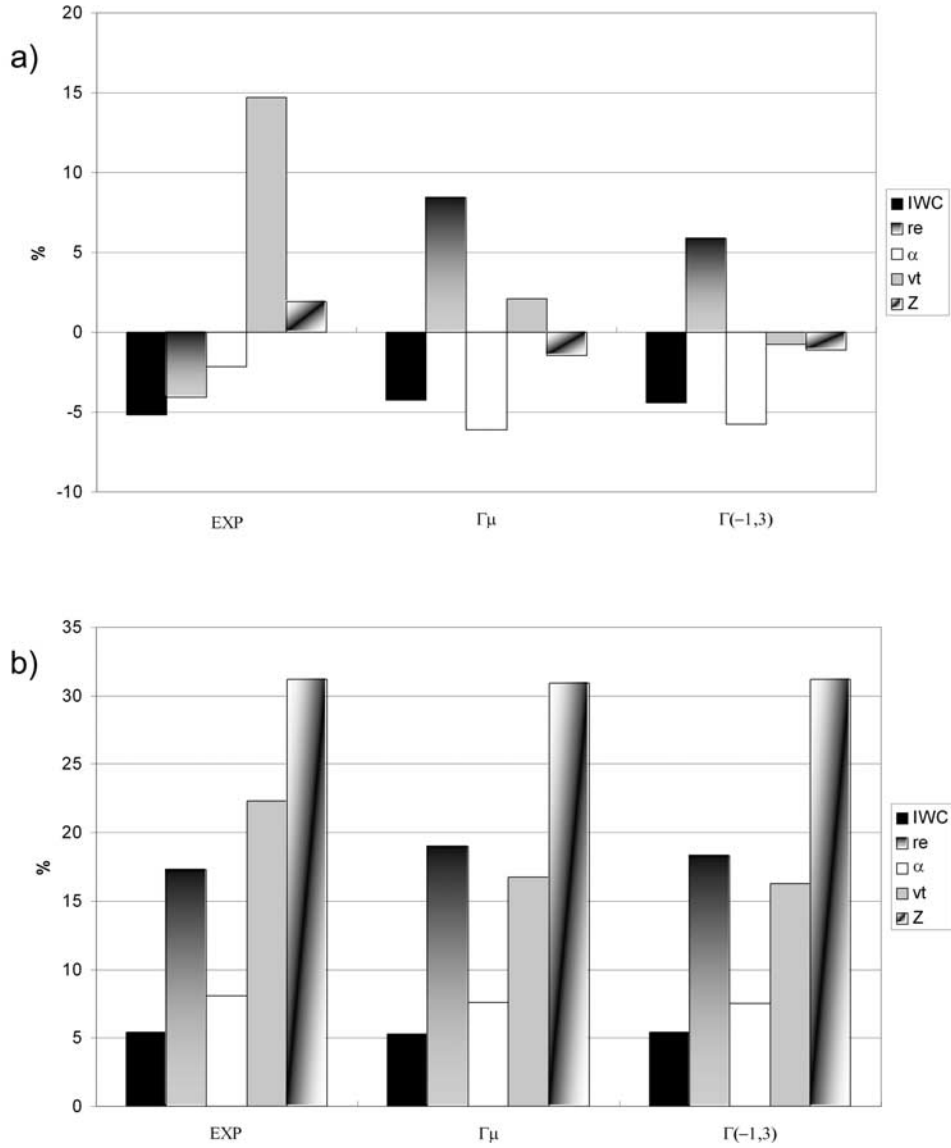

Figure 13. Assuming *Mitchell* [1996] hexagonal plates: (a) Mean relative error and (b) standard deviation on IWC, r_e, Z, V_t, α as a function of the following analytical PSD shapes: exponential, gamma with $\mu = 3$, and modified gamma shape.

relationships in the [−30°C; 0°C] interval. In climate models the particle time cannot be diagnosed from the model variables. Therefore we have derived a composite D_m-T relationship obtained from the three previously density relationships:

$$D_m = 1802.05 \exp[0.0326(T - 32.5)] \quad (27)$$

In order to estimate the potential of such a parameterization for the retrieval of the cloud parameters we have computed as in section 4.2.1 the cloud parameters using an analytical shape (exponential, and $\Gamma_m(-1,4)$), the "true" N_0^* and the D_m estimated from the D_m-T parameterization. The resulting mean relative error between "true" and estimated cloud parameters is quite large (200–300% standard deviation on the estimated cloud parameters), which indicates that such an estimate of D_m is not accurate enough to access the cloud properties using the normalized PSD approach.

[63] Currently, climate models used the *Kristjánsson et al.* [2000] relationship between the temperature and the mean maximum dimension $\overline{D}$ defined as:

$$\overline{D} = \frac{\int_0^\infty n(D) D dD}{\int_0^\infty n(D) dD} \quad (28)$$

where D is the maximum dimension of the ice particle.

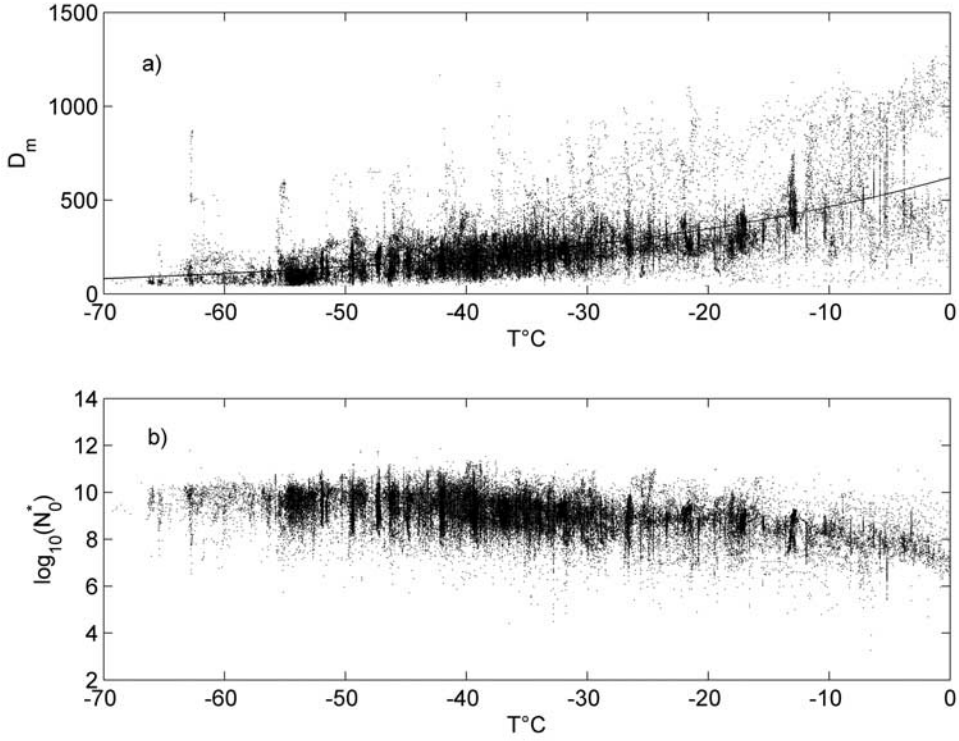

Figure 14. (a) D_m and (b) N_0^* as a function of temperature.

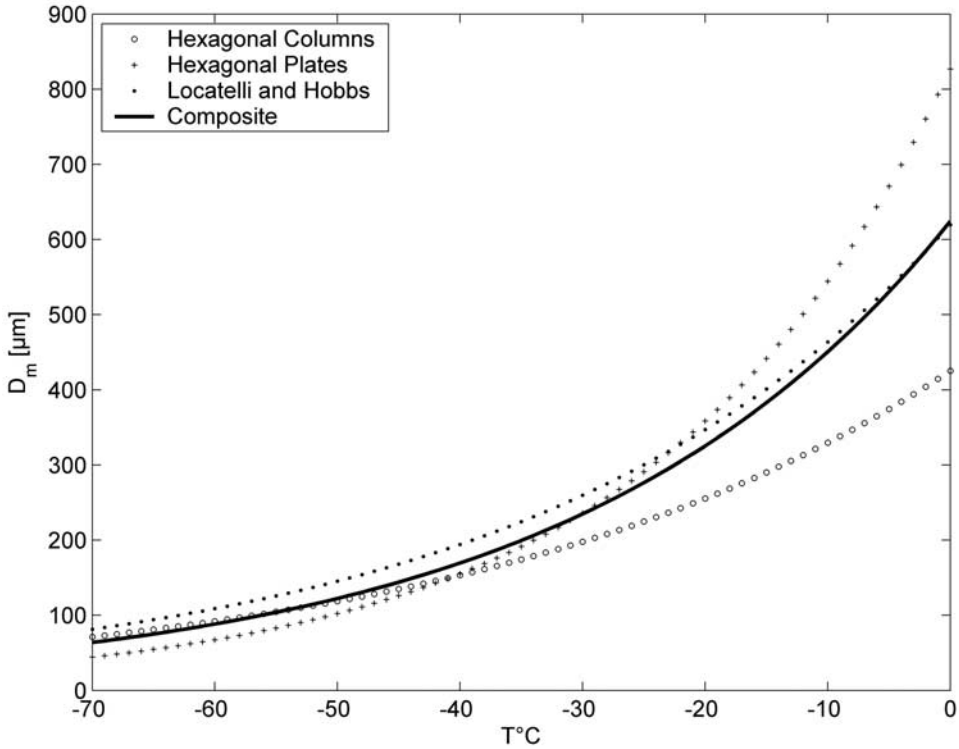

Figure 15. D_m as a function of temperature for three density/diameter relationships. The solid line is the relationship obtained from a mean exponential fit to the data for three density/diameter relationships (equations (24)–(27) in the text).

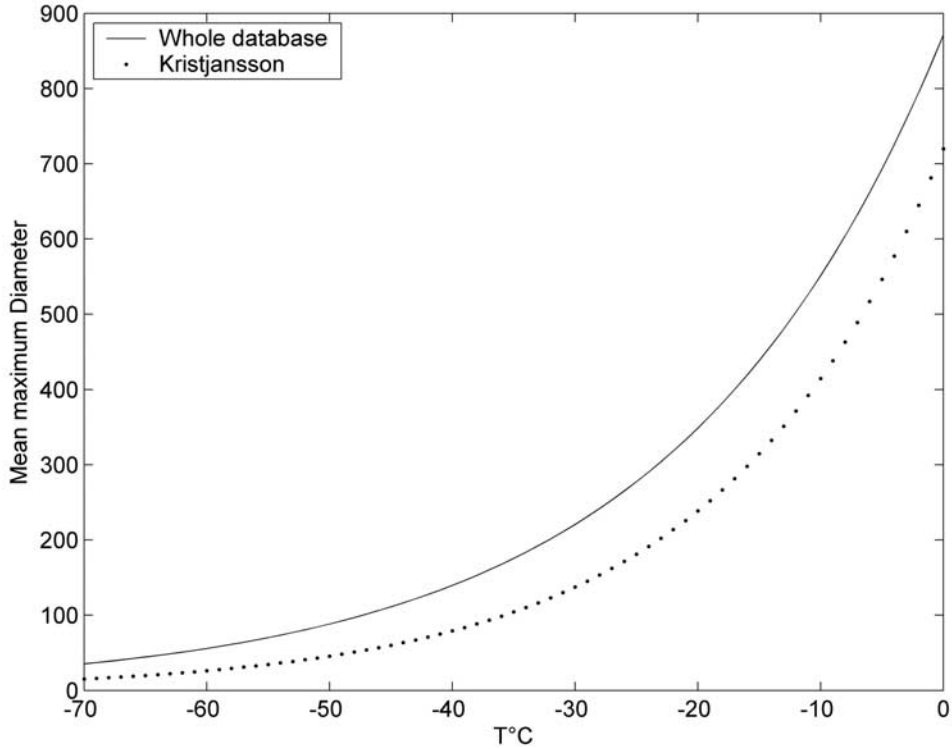

Figure 16. $\overline{D}$ as a function of temperature. The solid line is the relationship obtained from a mean exponential fit to the data (equation (29)), and the dotted line is the *Kristjánsson et al.* [2000] relationship currently used in the climate models.

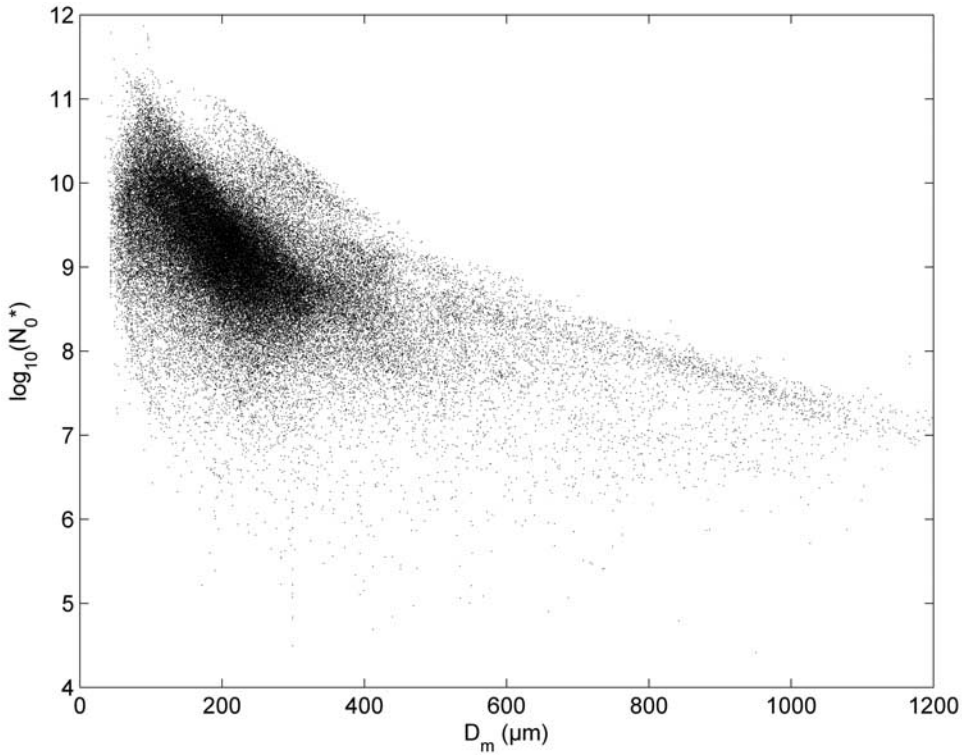

Figure 17. Scatterplot of log10(N_0^*) as a function of D_m (μm).

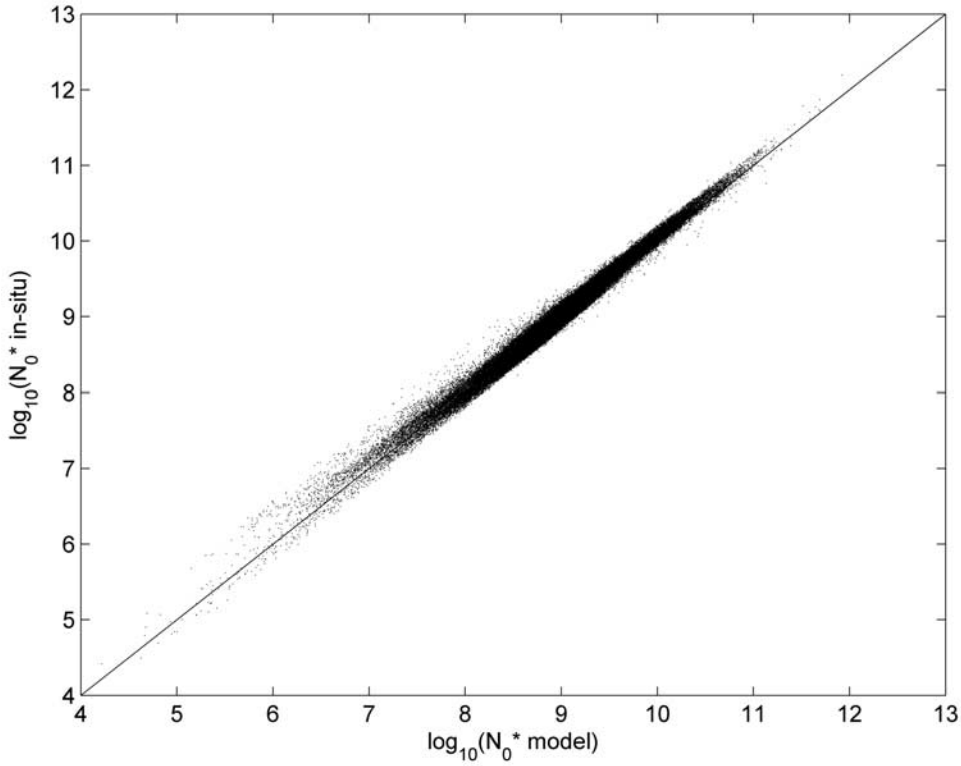

Figure 18. Scatterplot of N_0^* computed with the N_0^*-D_m-Z_e model with an exponential shape as a function of the true in situ N_0^*.

[64] As mentioned by *Kristjánsson et al.* [2000], this relationship appears statistically independent of the crystal type, which may be an advantage with respect to the previous D_m-T relationship. Since the *Kristjánsson et al.* [2000] relationship has been obtained using mostly the CEPEX in situ microphysical data, we have derived a $\overline{D}$-T relationship from our extensive database to evaluate this relationship:

$$\overline{D} = 97.8 \exp[0.0458(\mathrm{T} + 47.8)] \tag{29}$$

This relationship clearly produces larger mean maximum diameter than the formulation of *Kristjánsson et al.* [2000] currently used in climate models, as seen in Figure 16. This difference may be explained by the fact that the *Kristjánsson et al.* [2000] relationship has been obtained using a much smaller subset of in situ microphysical data, as discussed previously. The relationship of (29) is therefore believed to produce a better estimate of particle size at global scale, which could be useful to climate models.

5.2. Evaluation of N_0^* - D_m Relationships

[65] In the previous subsection we have seen that there was an opposite trend of N_0^* and D_m with temperature. However, relatively large errors are associated with parameterizations derived from these trends. Here we estimate the potential of using a single direct relationship between N_0^* and D_m. Figure 17 displays the scatter plot of $\log_{10}(N_0^*)$ versus D_m for all experiments. As for the parameterization of N_0^* by temperature, the variability of N_0^* covers six orders of magnitude for a given value of D_m, which translates into huge mean errors and standard deviations. We have then attempted to reduce these errors by splitting the dataset into different temperature intervals. Again, the error analysis (not shown) does not show any significant improvement of the errors when parameterizing the N_0^*-D_m relationship with temperature.

5.3. N_0^* - D_m Statistical Relationship Parameterized by Radar Reflectivity

[66] As seen previously, a single N_0^* - D_m relationship cannot be used to describe all normalized ice cloud PSDs. As a result further investigations are required to develop N_0^* - D_m relationships parameterized by a radar or a lidar observable. If such a relationship produces accurate N_0^* - D_m relationships, then it would imply that cloud parameters can be estimated with good accuracy from the estimate of only one parameter of the PSD (either N_0^* or D_m) and the radar or lidar observable. The radar reflectivity is a good candidate for this purpose, since in the Rayleigh regime, there is a straight relationship between N_0^* D_m and Z_e. As an example, in the case of the exponential shape this relationship can be written as

$$N_0^* = 4^7 \frac{|K_w|^2}{|K_i|^2} \left(\frac{\rho_i}{\rho_w}\right)^2 10^{18}\ \Gamma(7)^{-1} Z_e D_m^{-7} \quad \left(\mathrm{m}^{-4}\right) \tag{30}$$

where Z_e is in $\mathrm{mm}^6.\mathrm{m}^{-3}$ and D_m is in m, with $|K_i|^2 = 0.176$ at 94 GHz and $|K_w|^2 = 0.93$ at 3 GHz.

Table 2. Impact of the N_0^*-Ze-D_m Model on N_0^*, IWC, and α

	N_0^*		IWC		α	
	Relative Error, %	σ, %	Relative Error, %	σ, %	Relative Error, %	σ, %
Exp	−2.9	19.7	−2.9	19.7	−11.1	22
Gamma μ	−2.	15.7	−2.	15.7	−10.6	15
Gamma −1, 3	−3.	15.7	−3.	15.7	−11.7	13.4

[67] In the Mie regime, which occurs for radars at 94 GHz when particle diameters are greater than about 250 μm ($D > 0.08\ \lambda$ [*Battan*, 1973]), this relationship may be expressed as

$$N_0^* = \frac{|K_w|^2 \pi^5 10^{-18}}{\lambda^4} Z_e \ I(D_m)^{-1} \quad \left(\mathrm{m}^{-4}\right) \tag{31}$$

where $I(D_m)$ is an integral function of D_m and the normalized PSD shape. $I(D_m)$ is defined as:

$$I(D_m) = \int_{D_{\min}}^{D_{\max}} F\left(D_{eq}/D_m\right) \sigma_{bsc} dD_{eq} \tag{32}$$

In order to evaluate the errors associated with this N_0^*-D_m-Z_e model, we first compare in Figure 18 the true N_0^* computed directly from the measured PSDs and the N_0^* obtained with the N_0^*-D_m-Z_e model for exponential shape. It is to be noted that the different analytical shapes yield approximately the same results for N_0^*.

[68] The N_0^*-D_m-Z_e model produces a slight under-estimation of N_0^* (less than 3%) and the standard deviation does not exceed 16% for the gamma shapes, as seen in Table 2. This translates by definition into exactly the same error for IWC (Vt_Z and effective radius by definition do not depend on N_0^*), while the error is slightly larger for α but still reasonable (−10% bias and 15% standard deviation). It is important to mention here that this error analysis includes both the error contributions arising from the use of a single analytical shape and from the use of the N_0^*-D_m-Z_e model. This result implies that the cloud parameters can be estimated with this accuracy from the estimate of only one parameter of the PSD (N_0^* or D_m) and a radar reflectivity measurement.

6. Conclusion

[69] In the present paper, we have investigated the statistical properties of the normalized particle size distribution in ice clouds. To do so, an extensive database of airborne in situ microphysical measurements has been constructed and analyzed. Qualitatively, it is first obtained that there is a remarkable stability in shape of the normalized PSD for the normalized diameters D_{eq}/D_m smaller than 2, and a larger variability for larger diameters. A global analysis has therefore been conducted in order to assess the errors introduced on radar- and lidar-related parameters (reflectivity, specific attenuation, visible extinction) and cloud parameters (ice water content, effective radius, terminal fall velocity) derived by the use of a single analytical PSD shape for all the PSDs in the database instead of the "true" shape of each normalized PSD of the database. Different analytical shapes have been evaluated in this way. It has been obtained that the $\Gamma(-1, 4)$, $\Gamma(-1, 3)$ and $\Gamma_{\mu=3}$ shapes (see section 2 for definition) could be used as an accurate approximation for any normalized ice particle size distribution, and for any instrumental or cloud parameter to be derived from the normalized PSD. If the exponential shape is to be used, it has been found to be fairly accurate for ice water content, radar reflectivity and specific attenuation, and lidar extinction, but slightly less accurate for effective radius and reflectivity-weighted terminal fall velocity. It has also been demonstrated that these conclusions were valid for any particle type.

[70] The error analysis has also been conducted in 10°C temperature intervals, to check for potential systematic behaviour of the error on the cloud parameters as a function of temperature when using a single analytical shape for all ice cloud PSDs. No such behaviour has been found, which indicates that the proposed analytical shapes can be used with confidence at any temperature.

[71] This stability in shape and its unique analytical approximation implies that two parameters are now sufficient to describe any normalized PSD of ice clouds: N_0^* and D_m. We therefore investigated different possibilities to reduce again the number of unknowns by developing and evaluating statistical relationships (parameterizations) between N_0^* and D_m. Firstly, it has been shown that a parameterization of N_0^* and D_m by temperature could not be envisaged to retrieve the cloud parameters. Nevertheless, a D_m-T and a $\overline{D}$-T parameterization have been derived and compared to the parameterization of *Kristjánsson et al.* [2000] currently used to characterize particle size in climate models. The new parameterization generally produces larger particle sizes at any temperature than the *Kristjánsson et al.* [2000] parameterization. This new parameterization is believed to better represent particle size at global scale, owing to a better representativity of the in situ microphysical database.

[72] We have also estimated the errors that would arise from the use of a single N_0^*-D_m model to describe all normalized PSDs, parameterized either by temperature or radar reflectivity. While the model parameterized by temperature produces strong errors on the cloud parameters, the N_0^*-D_m model parameterized by radar reflectivity produces accurate cloud parameters (less than 3% bias and 16% standard deviation). This result implies that the cloud parameters can be estimated from only one parameter of the normalized PSD (N_0^* or D_m) and a radar reflectivity measurement. In a next paper, this method will be applied to the case of a vertically-pointing Doppler cloud radar. In this case, D_m can be estimated from the terminal fall velocity, which had been retrieved from the Doppler velocity.

[73] **Acknowledgments.** This work has been funded by Cnes and Alcatel, in the framework of the CALIPSO/CloudSat radar-lidar mission, and of the European Union CloudNet project under contract EVK2-CT-2000-00065. We are indebted to Robin Hogan from University of Reading, who provided us with processed EUCREX and CEPEX data sets.

References

Battan, L. J. (1973), *Radar Observation of the Atmosphere*, 325 pp., Univ. of Chicago Press, Chicago, Ill.

Best, A. (1950), The size distribution of raindrops, *Q. J. R. Meteorol. Soc.*, *76*, 16–36.

Brown, P. R. A., and P. N. Francis (1995), Improved measurements of the ice water content in cirrus using a total water probe, *J. Atmos. Oceanic Technol.*, *12*, 410–414.

Donovan, D. P., and A. C. A. P. van Lammeren (2001), Cloud effective particle size and water content profile retrievals using combined lidar and radar observations: 1. Theory and examples, *J. Geophys. Res.*, *106*, 27,425–27,448.

Ferreira, F., P. Amayenc, S. Oury, and J. Testud (2001), Study and tests of improved rain estimates from the TRMM precipitation radar, *J. Appl. Meteorol.*, *40*, 1878–1899.

Field, P., and A. J. Heymsfield (2003), Aggregation and scaling of ice crystal size distributions, *J. Atmos. Sci.*, *60*, 544–560.

Gaussiat, N., R. J. Hogan, and A. J. Illingworth (2004), Cloud water content and cloud particle characteristics revealed by dual wavelength cloud radar observations, paper presented at 14th International Conference on Clouds and Precipitation, Bologna, Italy.

Hu, Z., and R. C. Srivastava (1995), Evolution of raindrop size distribution by coalescence, breakup, and evaporation: Theory and observations, *J. Atmos. Sci.*, *52*(10), 1761–1783.

Intrieri, J. M., G. L. Stephens, W. L. Eberhard, and T. Uttal (1993), A method for determining cirrus cloud particle sizes using lidar and radar backscatter technique, *J. Appl. Meteorol.*, *32*(6), 1074–1082.

Kristjánsson, J. E., J. M. Edwards, and D. L. Mitchell (2000), The impact of a new scheme for the optical properties of ice crystals on the climates of two GCMs, *J. Geophys. Res.*, *105*, 10,063–10,079.

Law, J. O., and D. A. Parsons (1943), The relation of raindrop size to intensity, *Eos Trans. AGU*, *24*, 452–460.

Liu, C. L., and A. J. Illingworth (1999), Toward more accurate retrievals of ice water content from radar measurements of clouds, *J. Appl. Meteorol.*, *39*, 1130–1146.

Locatelli, J. D., and P. V. Hobbs (1974), Fall speed and masses of solid precipitation particles, *J. Geophys. Res.*, *79*, 2185–2197.

Marshall, J. S., and W. Palmer (1948), The distribution of raindrops with size, *J. Atmos. Sci.*, *5*(4), 165–166.

Matrosov, S. Y. (1996), Variability of microphysical parameters in high altitude ice clouds: Results of the remote sensing method, *J. Appl. Meteorol.*, *36*, 633–648.

McFarquhar, G. M., and A. J. Heymsfield (1998), The definition and significance of an effective radius for ice clouds, *J. Atmos. Sci.*, *55*, 2039–2052.

Mitchell, D. (1996), Use of mass- and area-dimensional power laws for determining precipitation particle terminal velocity, *J. Atmos. Sci.*, *53*, 1710–1723.

Stephens, G. L., S.-C. Tsay, P. W. Stackhouse, and P. J. Flatau (1990), The relevance of the microphysical and radiative properties of cirrus clouds to climate and climatic feedback, *J. Atmos. Sci.*, *47*(14), 1742–1754.

Testud, J., S. Oury, R. A. Black, P. Amayec, and X. K. Dou (2001), The concept of "normalized" distribution to describe raindrop spectra: A tool for cloud physics and cloud remote sensing, *J. Appl. Meteorol.*, *40*, 1118–1140.

Tinel, C., et al. (2005), The retrieval of ice cloud properties from cloud radar and lidar synergy, *J. Appl. Meteorol.*, in press.

Willis, P. T. (1984), Functional fits to some observed drop size distributions and parameterization of rains, *J. Atmos. Sci.*, *41*, 1648–1661.

A. Bansemer and A. J. Heymsfield, National Center for Atmospheric Research, Boulder, CO 80307, USA.

D. Bouniol, J. Delanoë, A. Protat, and J. Testud, Institut Pierre-Simon Laplace, Centre d'Etudes des Environnements Terrestres et Planétaires, UVSQ, 10-12 av. De l'Europe, 78140 Vélizy, France. (julien.delanoe@cetp.ipsl.fr)

P. R. A. Brown and R. M. Forbes, Meteorological Office, Reading RG12 2SZ, UK.